Available online at www.sciencedirect.com
SCIENCE DIRECT®
Journal of Solid State Chemistry 177 (2004) 2115–2121
JOURNAL OF SOLID STATE CHEMISTRY
http://elsevier.com/locate/jssc

The novel silicide Eu_3Si_4: structure, chemical bonding, magnetic behavior and electrical resistivity

Franz Weitzer,[a,b] Yurii Prots,[a] Walter Schnelle,[a] Kurt Hiebl,[b] and Yuri Grin[a,*]

[a] *Max-Planck-Institut für Chemische Physik fester Stoffe, Nöthnitzer Str. 40, D-01187 Dresden, Germany*
[b] *Institut für Physikalische Chemie, Universität Wien, Währingerstr. 42, 1090 Wien, Austria*

Received 10 November 2003; received in revised form 13 January 2004; accepted 1 February 2004

Abstract

The novel binary europium silicide Eu_3Si_4 was synthesized from the elements. Its crystal structure is a derivative of the Ta_3B_4 type: space group *Immm*, $a = 4.6164(4)$ Å, $b = 3.9583(3)$ Å, $c = 18.229(1)$ Å, $Z = 2$. In the structure, the silicon atoms form one-dimensional bands of condensed hexagons. Deviating from the prototype structure, a partial corrugation of the initially planar bands may be concluded from the analysis of the experimental electron density in the vicinity of the Si1 atoms. In the paramagnetic region, Eu_3Si_4 shows a $4f^7$ electronic configuration for the europium atoms. Two consecutive magnetic ordering transitions were found at 117 and 40 K. The first one is attributed to a ferromagnetic ordering of the Eu2 atoms; the second one is caused by a ferromagnetic ordering of the Eu1 atoms resulting in a ferrimagnetic ground state with a net magnetization of 7 μ_B at 1.8 K. The temperature dependence of the electrical resistivity reflects the metallic character of the investigated compound. Furthermore, the pronounced changes of the $d\rho/dT$ slope confirm the magnetic transitions. From bonding analysis with the electron localization function, Eu_3Si_4 shows a Zintl-like character and its electronic count balance can be written as $(Eu^{1.83+})_3(Si1^{0.95-})_2(Si2^{1.8-})_2$, in good agreement with its magnetic behavior in the paramagnetic region.

Keywords: Europium silicide; Crystal structure; Magnetic behavior; Electrical resistivity; Bonding analysis; Electron localization function

1. Introduction

A phase diagram for the binary system europium–silicon has not been established yet, but several binary phases were structurally characterized: Eu_5Si_3 (Cr_5B_3 type, space group *I*4/*mcm*) [1,2], EuSi (CrB type, space group *Cmcm*) [3–8], $EuSi_2$ (α-$ThSi_2$ type, space group $I4_1/amd$) [5–14] and, more recently, Eu_2Si (Co_2Si or anti-$PbCl_2$ type, space group *Pnma*) [15,16]. These silicides contain divalent europium and the chemical bonding is understood within the Zintl–Klemm concept. Loewenhaupt [5] reported the existence of another new binary silicide of the approximate composition Eu_4Si_5 with a hitherto unknown structure. We have recently started to investigate the ternary systems Eu–Si–B and Eu–Ge–B [17]. Thereby, a new, presumably binary compound was found. Hence we report on the synthesis, structure refinement, the chemical bonding and the magnetic properties of Eu_3Si_4.

2. Experimental

The samples with the nominal compositions $Eu_{38}Si_{62}$, $Eu_{43}Si_{57}$ and $Eu_{45}Si_{55}$, each with a total mass of approximately 1 g, were prepared by melting the appropriate amounts of the constituent elements (Eu, distilled prior to use, and Si 99.9999%) in a high-frequency furnace using a glassy carbon crucible. In the case of $Eu_{43}Si_{57}$, the reaction was performed in a sealed Ta crucible. After high-frequency melting, the reguli were wrapped in molybdenum foil, sealed in evacuated quartz tubes and annealed at 500°C for 5 months. Finally, all samples were quenched by submerging the quartz tubes into cold water. Owing to the high instability of the alloys against moisture and air, all handling of the specimens was performed in an argon-filled glove box system

*Corresponding author. Fax: +49-351-4646-3340.
E-mail address: grin@cpfs.mpg.de (Y. Grin).

0022-4596/$ - see front matter © 2004 Elsevier Inc. All rights reserved.
doi:10.1016/j.jssc.2004.02.013

ensuring an atmosphere with oxygen and H_2O levels lower than 1 ppm.

Phase identification and precise lattice parameter determination were performed with room temperature X-ray powder data using a Guinier image plate camera system Huber G670 (monochromatic Cu$K\alpha_1$ or Co$K\alpha_1$ radiation, $\lambda = 1.54056$ and 1.78896 Å, respectively; diffraction angle region $3° < 2\Theta < 100°$, step size 0.005° of 2Θ) employing an internal standard of 99.9999% pure Ge ($a = 5.657906$ Å). During the X-ray examination the powders were encapsulated in sealed Lindemann-glass capillaries or sealed between two polyimide foils.

Well-faced single crystals were separated by mechanical fragmentation of the Eu_3Si_4 sample. The quality of single crystals was checked by Laue photographs. A suitable crystal for X-ray data collection was mounted on a STOE IPDS. All crystallographic calculations were done with the Windows version of the CSD program package [18]. Details of the X-ray diffraction experiments and data handling are presented in Table 1.

The *dc* magnetization was measured in the temperature range 1.8–400 K and in applied magnetic fields up to 70 kOe using a superconducting quantum interference device (SQUID) magnetometer MPMS XL7 (Quantum Design). A *dc* Faraday pendulum magnetometer SUS-10 (A. Paar, Graz, Austria) in external fields up to 13 kOe has been applied for measurements at elevated temperatures (300–900 K).

Table 1
Crystallographic information and data handling for Eu_3Si_4

Composition	Eu_3Si_4
Space group	*Immm*
Pearson symbol	*oI*14
Formula units per unit cell (Z)	2
Unit-cell dimensions (powder data)	
a (Å)	4.6164(4)
b (Å)	3.9583(3)
c (Å)	18.229(1)
V (Å^3)	333.10(7)
Density (calculated) (g cm^{-3})	5.665(1)
Diffraction system	STOE IPDS
Radiation; wavelength λ (Å)	Ag$K\alpha$, 0.56087
Scan	225 images, $\Delta\varphi = 0.8°$
2θ range	$\leqslant 45°$
Range of hkl	$-6 \leqslant h \leqslant 6$
	$-5 \leqslant k \leqslant 5$
	$-24 \leqslant l \leqslant 24$
Measured reflections	1483
Independent reflections	276
R_{int}	0.076
Refl. with $F(hkl) > 4\,\sigma F(hkl)$	251
Absorption correction	Numerical, using crystal shape
Refinement mode	Full-matrix LS on $F(hkl)$
No. of refined parameters	18
Weighting scheme	Unit
Residuals $R(F)$ and w$R(F^2)$	0.032; 0.076

Electrical resistivity was measured by a standard *dc* four-probe technique (4–320 K) on an approximately rectangular polycrystalline piece of sample (estimated geometry factor error ±40%). For the measurements and handling the sample was kept all the time under argon/helium atmosphere or in vacuum.

3. Calculation procedure

The TB-LMTO-ASA program package [19] with exchange correlation potential (LDA) according to Barth and Hedin [20] was used for quantum chemical calculations. The radial scalar-relativistic Dirac equation was solved to get the partial waves. Although the calculation within the atomic sphere approximation (ASA) includes corrections for the neglect of interstitial regions and partial waves of higher order [21], an addition of empty spheres in case of Eu_3Si_4 was not necessary. The following radii of atomic spheres were applied for calculations: $r(Eu1) = 2.040$ Å, $r(Eu2) = 2.019$ Å, $r(Si1) = 1.516$ Å, $r(Si2) = 1.577$ Å. A basis set containing Eu(6*s*, 5*d*, 4*f*) and Si(3*s*, 3*p*) orbitals was employed for the self-consistent calculations with the Eu(6*p*) and Si(3*d*) functions being downfolded.

Two spin-polarized calculations were performed to explore the possible magnetic properties. In the first calculation the spins for both europium positions were parallel; in the second one the spins were considered as anti-parallel.

The electron localization function (ELF, η) was evaluated according to [22] with an ELF module already implemented within the TB-LMTO-ASA program package [19]. To gain a deeper insight into the chemical bonding, the topology of ELF was analyzed with the program Basin [23]. The electron density was integrated in basins, which are bounded by zero flux surfaces in ELF gradient. This method, analogous to the procedure proposed by Bader for the electron density [24], resulted for each basin in the electron counts, which reveal basic information for the description of the bonding situation.

4. Results and discussion

4.1. Structure chemistry

A phase analysis of the prepared samples revealed the following phase equilibria in the binary system Eu–Si. The sample $Eu_{38}Si_{62}$ contained Eu_3Si_4 phase together with small amounts of europium disilicide, and $Eu_{45}Si_{55}$ showed Eu_3Si_4 in equilibrium with europium monosilicide. Only the alloy with the nominal composition $Eu_{43}Si_{57}$ was found to be a single-phase one. The lattice parameters of the Eu_3Si_4 phase were determined for all three samples prepared and vary in the following ranges

with increasing silicon content: $a = 4.6242(6) - 4.6121(6)$ Å, $b = 3.9518(5) - 3.9575(6)$ Å, and $c = 18.241(3) - 18.236(2)$ Å. Thereby the a value varies monotonically with concentration, the b parameter achieves a maximal value and the c parameter exhibits a minimum at the composition Eu_3Si_4 (cf. Table 1). The results above prove the existence of a narrow homogeneity range around the composition 3:4. The structural reasons for the formation of a homogeneity range can be a partial multiple substitution of europium atoms by silicon similarly to $Eu_{2-x}Ga_{3+2x}$ [25] or $Eu_{3-x}Ga_{8+3x}$ [26]. The extremely small concentration range does not allow a specification of the mechanism in detail.

A detailed analysis of the single-crystal diffraction data (see Fig. 1) showed two diffracting domains, which were integrated practically without overlapping. Thereby we received two data sets, which were of equal quality. Each data set (Laue class *mmm*) revealed systematic extinctions corresponding to the extinction symbol *I*---. From the possible space groups *Immm*, *Imm*2 and *I*222, the centre-symmetric *Immm* was chosen for further structure solution and refinement. The structure was solved by direct methods and refined with an anisotropic approximation of atomic displacement for all atoms. At this stage, the Si1 atoms exhibited a strong anisotropy: $B_{11} \gg B_{22} \approx B_{33}$ suggesting a local symmetry breaking caused by slight displacement of the Si1 atoms out of the mirror plane. In the final refinement, a split position was applied for the description of the electron density in this region. Final atomic coordinates together with anisotropic displacement parameters are presented in Table 2, the according interatomic distances are listed in Table 3.

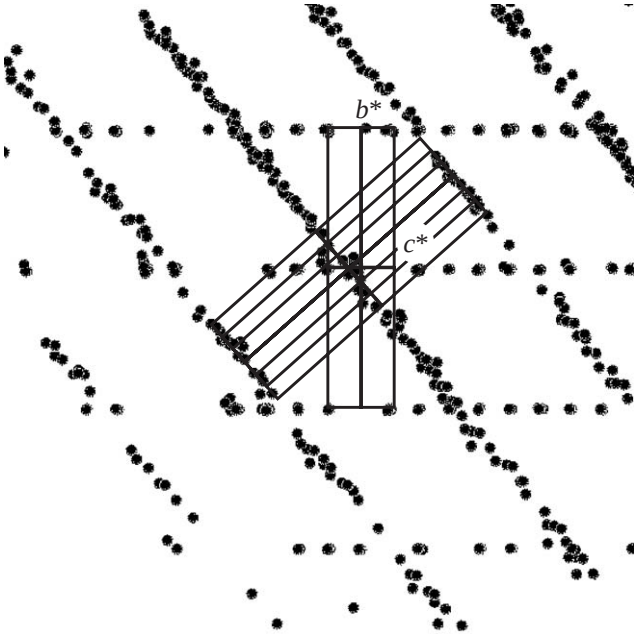

Fig. 1. Two diffracting domains of the Eu_3Si_4 crystal: total projection of the diffraction space along the a^* direction of the domain I.

The crystal structure of Eu_3Si_4 is a new binary representative of the structure type Ta_3B_4 [27] or its ternary ordering variant $Ca_3Al_2Ge_2$ [28]. In the ideal structure, the silicon atoms form planar one-dimensional bands built of condensed Si_6 hexagons. The hexagons are formed by three-bonded Si1(3b) and two-bonded Si2(2b) atoms. The europium atoms are sandwiched between the bands, either in front of the hexagons or on their periphery. The neighboring 'sandwiches' are shifted by $(\frac{11}{22}0)$ relative to each other causing the body-centred translation symmetry (Fig. 2, upper part). The shift of the Si1 atoms out of the mirror plane can be interpreted as deformation of the flat silicon hexagons either toward a chair-like conformation (Fig. 2, lower part, right or left) or toward a boat-like one (Fig. 2, lower part, middle). This local conformation change might be caused, e.g., by the possible triple replacement of europium by silicon atoms. Similar gallium/europium replacement in $Eu_{2-x}Ga_{3+2x}$ [25] leads to a displacement of the gallium atoms adjacent to the implemented Ga_3 triangle from the ideal positions in the plane hexagon net. Another possibility for this kind of corrugation may be an instability of the planar hexagon nets for electronic reasons, similar to the

Table 2
Atomic coordinates and anisotropic displacement parameters (Å^2) for the crystal structure of Eu_3Si_4

Atom	Site	x/a	y/b	z/c	B_{11}[a]	B_{22}	B_{33}	B_{eq}[b]
Eu1	2*a*	0	0	0	0.50(6)	0.52(5)	0.51(6)	0.51(3)
Eu2	4*j*	1/2	0	0.31500(6)	0.55(4)	0.52(4)	0.55(4)	0.54(2)
Si1[c]	8*m*	0.022(3)	0	0.4360(4)	0.9(3)	0.6(2)	0.3(2)	0.6(1)
Si2	4*j*	1/2	0	0.1377(3)	1.0(2)	0.5(2)	0.6(2)	0.7(1)

[a] $B_{12} = B_{13} = B_{23} = 0$ for all positions.
[b] B_{eq} is defined as $[B_{11}a^{*2}a^2 + \cdots + 2B_{23}b^*c^*bc\cos\alpha]/3$.
[c] Occupancy: 0.5 Si.

Table 3
Interatomic distances (<3.968) in the structure of Eu_3Si_4

Atoms	Distance	Atoms	Distance
Eu1–8Si1	3.19(1)[a]	Si1–1Si1	2.335(11)[a]
	3.33(1)[a]		2.344(11)[a]
Eu1–4Si2	3.410(5)	Si1–2Si2	2.394(6)
Eu1–4Eu2	3.910(1)	Si1–1Eu2	3.12(1)
Eu1–2Eu1	3.9583(3)	Si1–2Eu1	3.19(1)
Eu2–2Si1	3.12(1)[a]	Si1–1Eu2	3.27(1)
	3.27(1)[a]	Si1–2Eu1	3.33(1)
Eu2–4Si2	3.160(2)	Si2–4Si1	2.394(6)
Eu2–1Si2	3.232(6)	Si2–4Eu2	3.160(2)
Eu2–4Eu2	3.855(1)	Si2–1Eu2	3.232(6)
Eu2–2Eu1	3.910(1)	Si2–2Eu1	3.410(5)
Eu2–2Eu2	3.9583(3)		

[a] Alternating distances.

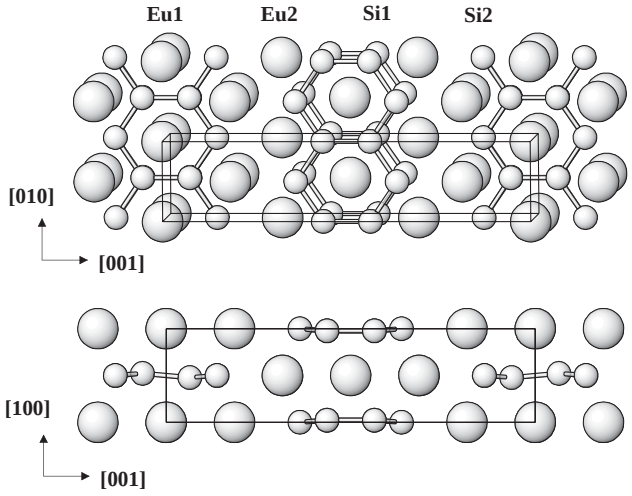

Fig. 2. Crystal structure of Eu_3Si_4: (upper part) view along [100] with one-dimensional bands of condensed Si_6 hexagons; (lower part) projection along [010] with possible conformations of the hexagons caused by displacement of the Si1 atoms in the real structure.

ytterbium digallide (corrugated nets) in comparison with digallides of the light rare-earth metals (planar nets) [29].

4.2. Magnetism and electrical resistivity

The results of the magnetization measurements are presented in Figs. 3–5. In the paramagnetic regime, the reciprocal susceptibility H/M depends almost linearly from temperature as shown in Fig. 3 and hence the experimental data were fitted within the temperature range $200\,K < T < 900\,K$ according to a Curie–Weiss law $\chi = C(T-\theta)^{-1}$, where C is the Curie constant and θ is the paramagnetic Curie temperature. From the non-linear least-squares calculation an effective paramagnetic moment $\mu_{eff} = 7.93(3)\,\mu_B$ per Eu atom, which is a clear indication for a ground state $^8S_{7/2}$ ($L = 0$) of europium in $4f^7$ electronic configuration (Eu^{2+}), was derived together with a positive value of $\theta = 102(1)\,K$.

The temperature dependence of the magnetization for various applied fields ($H = 100\,Oe$, 1 kOe and 10 kOe) is revealed in Fig. 4. All three curves show a strong increase at the Curie temperature of $T_C = 117\,K$ (determined from the steep rise in the 100 Oe data) due to a ferromagnetic order of the Eu sublattice. In both moderate fields the magnetization curves tend to saturate below $\approx 100\,K$ (plateau), start to rise again and pass maxima around 25 K. On the other hand, the magnetization in $H = 10\,kOe$ passes a broader maximum at $\approx 50\,K$, shows a weak shoulder at $\approx 25\,K$ and reaches a value of magnetization $M = 7\,\mu_B$/f.u. at $T = 1.8\,K$. The curves of isothermal magnetization vs. applied field at two temperatures, 1.8 and 75 K (Fig. 5), show the typical features of a simple isotropic "ferro-

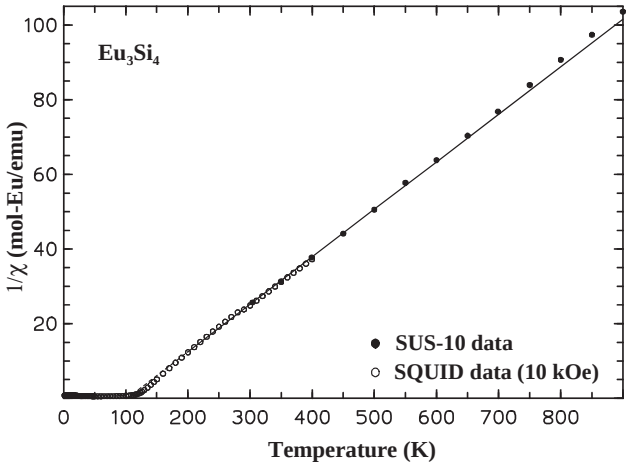

Fig. 3. Reciprocal magnetic susceptibility vs. temperature for Eu_3Si_4.

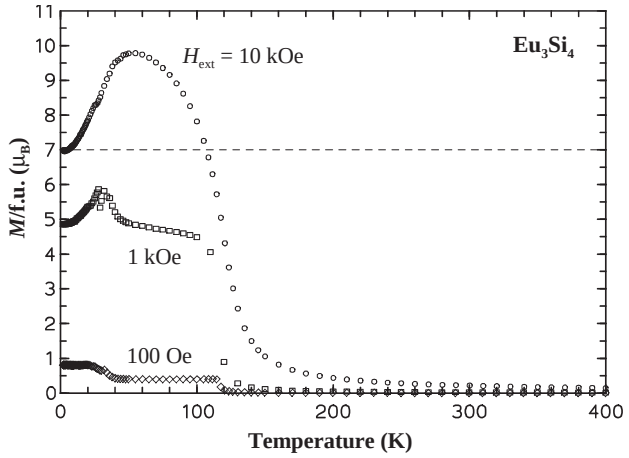

Fig. 4. Magnetization vs. temperature in three different applied magnetic fields for Eu_3Si_4.

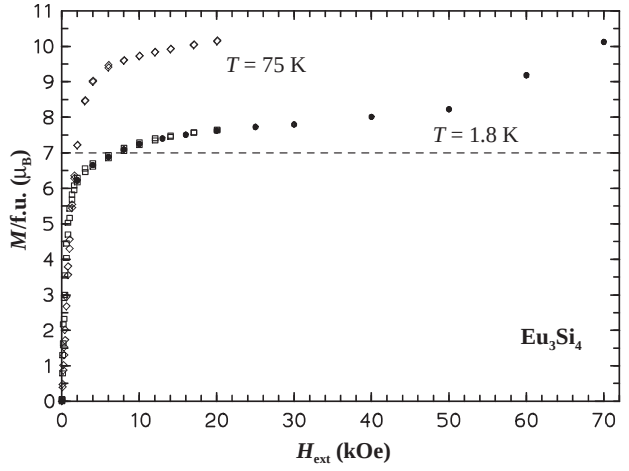

Fig. 5. Isothermal magnetization vs. applied field at 1.8 and 75 K for Eu_3Si_4. Different symbols for $T = 1.8\,K$ show results of two different measurements.

magnet''. However, it has to be emphasized that the higher value of the saturation magnetization ($M \approx 10\,\mu_B$/f.u.) is achieved at the higher temperature. We interpret these observations in the following way: Eu_3Si_4 undergoes two consecutive ferromagnetic phase transitions. At $T_C = 117$ K the two Eu2 atoms per formula unit residing at the crystallographic position ($\frac{1}{2}$ 0 0.315) order spontaneously, whereas the remaining one Eu1 atom per f.u. forms an ordered sublattice below 40 K. Upon lowering the temperature ($T < 50$ K), these two sublattices gradually align anti-parallel giving rise to a ferrimagnetic ground state (two spins up and one down per formula unit) at 0 K. This assumption is corroborated by the saturation moment of $\mu_S = 7\,\mu_B$/f.u. $= gJ$ found at 1.8 K. The expected sublattice moment of $14\,\mu_B$/f.u. stemming from the ferromagnetic Eu2 atoms can be estimated from an extrapolation of the $M(T)$ curve in a magnetic field of 10 kOe down to 0 K. Hence, the higher net saturation magnetization found at 75 K is plausible. The pronounced upturn of the magnetization plot at $T = 1.8$ K in fields above $H > 50$ kOe has to be attributed to a break-up of the ferrimagnetic spin alignment. This rather simple interpretation is also supported by the theoretical calculation below, which energetically favor the ferrimagnetic ground state.

The temperature dependence of the electrical resistivity $\rho(T)$ and its derivative $d\rho/dT$ are given in Fig. 6. Above 130 K $\rho(T)$ is linear dependent on T (metal-like behavior, cf. the results of the band structure calculations, Chapter 4.3) and reaches 5.3 mΩ cm at 300 K. This value is unusually large, even for silicides, however, the major part (3.4 mΩ cm; derived from a linear extrapolation to $T = 0$ from above 130 K) is due to the magnetic disorder scattering. A large magnetic skew scattering is expected for Eu_3Si_4 due to the maximum deGennes factor of Eu^{2+} among the rare earth ions and its large Eu content. The derivative $d\rho/dT$, which often shows

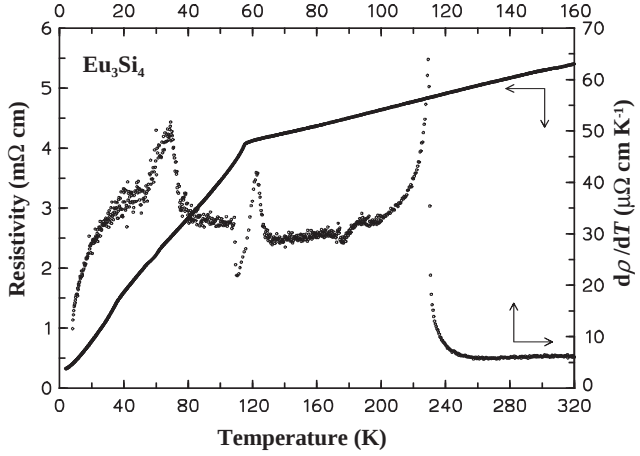

Fig. 6. Electrical resistivity $\rho(T)$ and derivative $d\rho/dT$ for Eu_3Si_4. The ''zigzag'' anomaly in $d\rho/dT$ at around 60 K is an artifact due a strongly varying heating rate (dwindling helium flow).

the features of the magnetic contribution to the heat capacity, provides further information. The ferromagnetic ordering gives a typical large λ-shaped (due to critical effects) anomaly in $d\rho/dT$ with a sharp peak at 115(1) K. Besides this transition, the peak at ≈ 30 K in the magnetization curve at $H_{ext} = 1$ kOe (see Fig. 4) is mirrored by an anomaly of complex shape in $d\rho/dT$ with a maximum at 35(1) K.

4.3. Chemical bonding and electronic density of states

The iso-stoichiometric compounds R_3Si_4 and R_3Ge_4 were found for R = Ca, Sr and Ba. All of them reveal polyanions formed from two- and three-bonded atoms in the 1:1 ratio and, therefore, can be easily formulated in sense of the Zintl–Klemm concept. Unlike the title europium silicide with *two-dimensional* silicon bands, Ca_3Si_4 shows a *three-dimensional* network of three- and two-bonded silicon atoms with calcium atoms embedded. The electronic count for this compound is formulated as $(Ca^{2+})_9(Si^{1-})_6(Si^{2-})_6$ [30]. On the other hand, the crystal structure of Ba_3Si_4 is formed by *isolated* four-atomic butterfly V-like silicon clusters with three- and two-bonded atoms, and can also be written as $(Ba^{2+})_6(Si^{1-})_2(Si^{2-})_2$ [31]. The homologous germanide Ba_3Ge_4 forms a crystal structure containing both, *isolated* four-atomic groups (3b- and 2b-germanium atoms) and *one-dimensional* polyanions built of 3b- and 2b-atoms: $(Ba^{2+})_6[(Ge^{1-})_2(Ge^{2-})_2]^1_\infty[(Ge^{1-})_2(Ge^{2-})_2]$ [32]. Among the R_3Si_4 and R_3Ge_4 compounds, only the strontium germanide Sr_3Ge_4 forms the structure of the same type as Eu_3Si_4 [33].

Following the Zintl–Klemm concept and taking into account the presence of three- and two-bonded silicon atoms in the structure, Eu_3Si_4 may be written in sense of formal oxidation state as $(Eu^{2+})_3(Si1^{1-})_2(Si2^{2-})_2$. More detailed insight into the chemical bonding was achieved with the electron localization function. The topology of the total ELF (calculated for the anti-parallel spin configuration for the two crystallographically independent europium positions and for the non-displaced Si2 position with the Si1 position as from the structure determination) reveals some features in the valence region in vicinity of the silicon atoms. Inherent ELF attractors can be ascribed to the bonds Si1–Si1 and Si1–Si2 in the silicon hexagon bands. Integration of the total electron density in the basins of these attractors gives electron counts of 2.1 and 1.7 for Si1–Si1 and Si1–Si2, respectively. Two additional attractors with the electron count of 1.1 each can be found above and below the Si1 atoms suggesting a 'lone-pair'-like behavior with geometrical p character for the three-bonded atoms in a planar configuration (Fig. 7, upper part). The two-bonded Si2 atoms also have two attractors above and below the hexagon band plane, which can be attributed to 'lone-pairs' (electron count of 2.0 for each, Fig. 7,

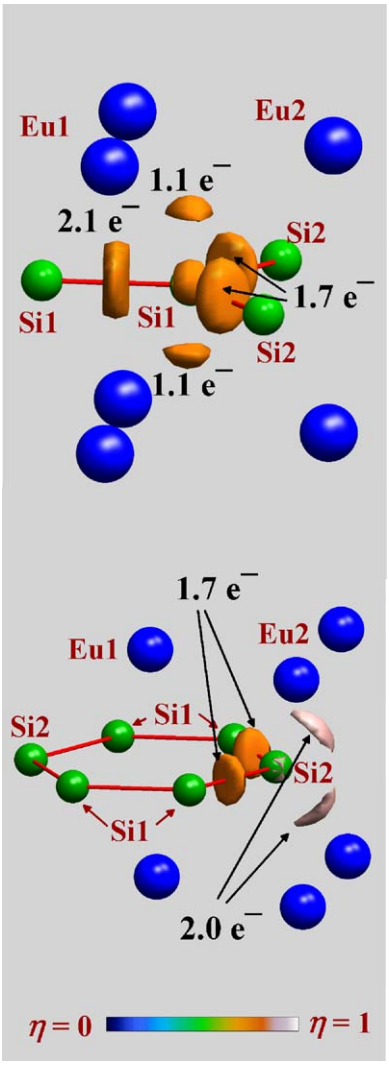

Fig. 7. Electron localization function in the Eu_3Si_4 structure: (upper part) isosurface with $\eta = 0.780$ showing the bonding attractors for Si1–Si1 and Si1–Si2 bonds and the 'lone-pair' *p*-like attractors for Si1 atoms; (lower part) isosurface with $\eta = 0.857$ (rose) showing 'lone-pair' attractors in the vicinity of Si2 atoms together with the bonding attractors in the silicon bands represented by isosurface with $\eta = 0.8$ (orange). The black labels give the electron counts for each basin.

lower part). Assuming homolytic cleavage of the electron counts in the silicon bonds, and attributing the 'lone-pair' counts to the according atoms, the silicon atoms achieve the formal oxidation states of −0.95 for Si1 and −1.8 for Si2. The total electronic count balance for the anionic part of the Eu_3Si_4 structure is, consequently, $(Si1^{0.95-})_2(Si2^{1.8-})_2$ which requires the formal count of 1.83+ for the europium atoms. The last fact correlates well with the f^7 electronic configuration found from the magnetic properties. The donating behavior of the europium atoms is confirmed by the following features in the topology of ELF. The inner shell is non-structured, which suggests that the inner-shell electrons do not participate in the interaction in the valence region [34]. The basins in the valence shell interconnect at the high value of $\eta = 0.68$ to one polyanion shell basin; the basin of the europium inner shell interconnects with the polyanion basin only at very low value of $\eta < 0.1$.

The electronic density of states for Eu_3Si_4 confirms the bonding analysis with ELF. The DOS in the valence region ($E < -2$ eV) is governed by the *s* and *p* states of silicon together with the *s* states of europium. The *f* states of europium dominate in the vicinity of the Fermi level, and result in a significant density of states at E_F (Fig. 8, top), which explains the metal-like temperature dependence of the electrical resistivity (cf. Fig. 6). According to the ferromagnetic ground state, the most

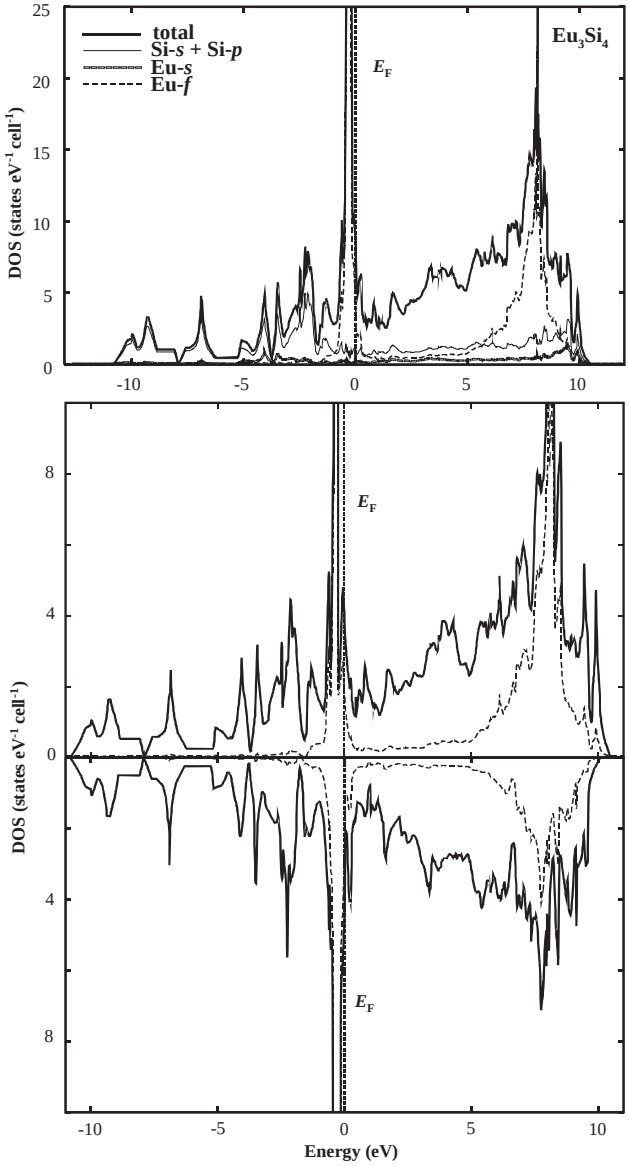

Fig. 8. Electronic density of states for Eu_3Si_4 with the partial contributions of selected silicon and europium states (top) and spin-resolved DOS with partial contributions of europium *f* states (bottom).

differences in the spin-resolved DOS are caused by f states of europium (Fig. 8, bottom).

A comparative calculation of the ferro- and ferrimagnetic ordering of the Eu1 and Eu2 positions shows that the latter state has a slightly lower total energy at 0 K ($\Delta E = 2$ mRy) which correlates with the magnetic observations (cf. Figs. 4 and 5).

After submitting the paper for publication we received information about an independent investigation on Eu_3Si_4 [35]. The structure determination performed on a single crystal selected from the barium-containing ternary sample revealed a strong anisotropy for the Si1 position. Temperature dependence of the magnetization showed two special features similar to our results.

5. Summary

The novel binary silicide Eu_3Si_4 possesses a structure derived from the Ta_3B_4 type. Deviating from the prototype with planar boron substructure, the silicon atoms form partially corrugated one-dimensional bands of condensed hexagons. Bonding analysis with electron localization function shows a Zintl-like behavior with the electronic count balance $(Eu^{1.83+})_3(Si1^{0.95-})_2(Si2^{1.8-})_2$ in good accord with the magnetization measurements revealing the $4f^7$ electronic configuration in the paramagnetic state. Below two ferromagnetic ordering transitions, Eu_3Si_4 has a ferrimagnetic spin structure at low temperatures. Measurement of the electrical resistivity proofs the metallic character of Eu_3Si_4 in good accordance with the band structure calculation.

References

[1] R. Pöttgen, R.-D. Hoffmann, D. Kuβmann, Z. Anorg. Allg. Chem. 624 (1998) 945.
[2] E.A. Leon-Escamilla, J.D. Corbett, J. Solid State Chem. 159 (2001) 149.
[3] E.I. Gladyshevskii, P.I. Kripyakevich, J. Struct. Chem. 5 (1964) 789.
[4] F. Merlo, M.L. Fornasini, J. Less-Common Met. 13 (1967) 603.
[5] M. Loewenhaupt, Z. Phys. 267 (1974) 219.
[6] A.A. Dakhel, Jpn. J. Appl. Phys. (Part 1) 21 (1982) 1521.
[7] A.A. Dakhel, Jpn. J. Appl. Phys. (Part 1) 21 (1982) 1101.
[8] A.A. Dakhel, Acta Phys. Pol. 70 (1986) 791.
[9] I. Binder, J. Am. Ceram. Soc. 43 (1960) 287.
[10] I. Mayer, I. Shidlovsky, E. Yanir, J. Less-Common Met. 12 (1967) 46.
[11] I. Shidlovsky, I. Mayer, J. Phys. Chem. Solids 30 (1967) 1207.
[12] J. Evers, G. Oehlinger, A. Weiss, J. Solid State Chem. 20 (1977) 173.
[13] R. Nesper, H.G. von Schnering, J. Curda, Solid Compounds of Transition Elements, VI International Conference, Abstracts, Stuttgart, 1979, p. 150.
[14] J. Evers, G. Oehlinger, A. Weiss, F. Hulliger, J. Less-Common Met. 90 (1983) L19.
[15] R. Mishra, R.-D. Hoffmann, R. Pöttgen, H. Trill, B.D. Mosel, Z. Anorg. Allg. Chem. 628 (2002) 741.
[16] F. Merlo, A. Palenzona, M. Pani, J. Alloys Compd. 348 (2003) 173.
[17] F. Weitzer, W. Schnelle, R. Cardoso Gil, Yu. Prots, Yu. Grin, Proceedings of the 14th International Symposium on Boron, Borides and Related Compounds (ISBB '02), Program and Abstracts, St. Petersburg, Russia, 2002, p. O2.
[18] L.G. Akselrud, P.Yu. Zavalii, Yu.N. Grin, V.K. Pecharski, B. Baumgartner, E. Wölfel, Mater. Sci. Forum 133–136 (1993) 335.
[19] O. Jepsen, A. Burkhardt, O.K. Andersen, The Program TB-LMTO-ASA. Version 4.7, Max-Planck-Institut für Festkörperforschung, Stuttgart, 1999.
[20] U. Barth, L. Hedin, J. Phys. C 5 (1972) 1629.
[21] O.K. Andersen, Phys. Rev. B 12 (1975) 3060.
[22] A. Savin, H.J. Flad, J. Flad, H. Preuss, H.G. von Schnering, Angew. Chem. 104 (1992) 185;
A. Savin, H.J. Flad, J. Flad, H. Preuss, H.G. von Schnering, Angew. Chem. Int. Ed. Engl. 31 (1992) 185.
[23] M. Kohout, Basin, Version 2.3, Max-Planck-Institut für Chemische Physik fester Stoffe, Dresden, 2001.
[24] R.F.W. Bader, Atoms in Molecules: A Quantum Theory, Oxford University Press, Oxford, 1999.
[25] O. Sichevych, R. Ramlau, M. Schmidt, R. Niewa, W. Schnelle, H. Borrmann, Yu. Grin, 2004, to be published.
[26] O. Sichevych, Yu. Prots, W. Schnelle, R. Niewa, D. Zherebtsov, R. Ramlau, Yu. Grin, 2004, to be published.
[27] R. Kiessling, Acta Chem. Scand. 3 (1949) 603.
[28] A. Widera, B. Eisenmann, H. Schäfer, K. Tuban, Z. Naturforsch. 31B (1976) 1592.
[29] U. Schwarz, R. Giedigkeit, R. Niewa, M. Schmidt, W. Schnelle, R. Cardoso, M. Hanfland, Z. Hu, K. Klementiev, Yu. Grin, Z. Anorg. Allg. Chem. 627 (2001) 2249.
[30] P. Manfrinetti, M.L. Fornasini, A. Palenzona, Intermetallics 8 (2000) 223.
[31] B. Eisenmann, K.H. Janzon, H. Schäfer, A. Weiss, Z. Naturforsch. 24B (1969) 457.
[32] F. Zürcher, R. Nesper, Angew. Chem. Int. Ed. 37 (1998) 3314.
[33] H. Schäfer, B. Eisenmann, W. Müller, Angew. Chem. 17 (1973) 742.
[34] M. Kohout, F.R. Wagner, Yu. Grin, Theor. Chem. Acc. 108 (2002) 150.
[35] M.E. Spahr, R. Nesper, Unpublished results, 1997; M.E. Spahr. Synthese und Charakterisierung neuartiger Oxide, Kohlenstoffverbindungen, Silizide sowie nanostrukturierter Materialien und deren elektro- und magnetochemische Untersuchung. Ph.D. Thesis, ETH Zürich, Switzerland, 1997.